Ultraflexible, large-area, physiological temperature sensors for multipoint measurements

Tomoyuki Yokota[a,b,1,2], Yusuke Inoue[a,b,1], Yuki Terakawa[a], Jonathan Reeder[a,c], Martin Kaltenbrunner[a,b], Taylor Ware[d], Kejia Yang[e], Kunihiko Mabuchi[f], Tomohiro Murakawa[g], Masaki Sekino[a,b], Walter Voit[c], Tsuyoshi Sekitani[a,b,h], and Takao Someya[a,b,2]

[a]Electrical and Electronic Engineering and Information Systems, The University of Tokyo, Bunkyo-ku, Tokyo 113-8656, Japan; [b]Exploratory Research for Advanced Technology, Japan Science and Technology Agency, Bunkyo-ku, Tokyo 113-8656, Japan; [c]Department of Materials Science and Engineering, The University of Texas at Dallas, Richardson, TX 75080-3021; [d]Department of Bioengineering, The University of Texas at Dallas, Richardson, TX 75080-3021; [e]Department of Chemistry, The University of Texas at Dallas, Richardson, TX 75080-3021; [f]Information Science and Technology, The University of Tokyo, Bunkyo-ku, Tokyo 113-8656, Japan; [g]Department of Cardiothoracic Surgery, The University of Tokyo Hospital, Bunkyo-ku, Tokyo 113-8655, Japan; and [h]The Institute of Scientific and Industrial Research, Osaka University, Ibaraki, Osaka 567-0047, Japan

Edited by John A. Rogers, University of Illinois, Urbana, IL, and approved September 28, 2015 (received for review August 7, 2015)

We report a fabrication method for flexible and printable thermal sensors based on composites of semicrystalline acrylate polymers and graphite with a high sensitivity of 20 mK and a high-speed response time of less than 100 ms. These devices exhibit large resistance changes near body temperature under physiological conditions with high repeatability (1,800 times). Device performance is largely unaffected by bending to radii below 700 μm, which allows for conformal application to the surface of living tissue. The sensing temperature can be tuned between 25 °C and 50 °C, which covers all relevant physiological temperatures. Furthermore, we demonstrate flexible active-matrix thermal sensors which can resolve spatial temperature gradients over a large area. With this flexible ultrasensitive temperature sensor we succeeded in the in vivo measurement of cyclic temperatures changes of 0.1 °C in a rat lung during breathing, without interference from constant tissue motion. This result conclusively shows that the lung of a warm-blooded animal maintains surprising temperature stability despite the large difference between core temperature and inhaled air temperature.

flexible electronics | organic electronics | biomedical devices | temperature sensor

Temperature control plays a very important role in homeostasis, and body temperature varies both spatially and temporally in an effort to transfer heat between the living body and the environment via skin and respiratory organs. Accurate measurement of localized temperature changes in soft tissue regardless of large-scale motion is important in understanding thermal phenomena of homeostasis and realizing future sophisticated health diagnostics (1–3). Therefore, flexible temperature sensors which softly interface with tissue have been investigated frequently for applications in the medical field. However, these applications require the combination of sensitivity, fast response time, stability in physiological environments, and multipoint measurement. Before this work, to our knowledge, no experiment has simultaneously demonstrated orders-of-magnitude changes in electrical properties (sensitivity) repeatedly at varying physiological temperatures and conditions (stability) in a robust, easy-to-fabricate, flexible temperature sensor (processability).

When sensors and electronics are directly attached to the surface of an animal body, the use of soft and flexible electronic devices is expected to reduce mechanical stress induced on the body. From this viewpoint, the field of flexible electronics has attracted much attention recently. The ability to gather information such as pressure and temperature from curvilinear and dynamic surfaces without impairing the movement or usability of the users is unmatched by conventional silicon electronics. There have been reports of the potential application of flexible electrodes on ultrathin substrates (4), flexible sensors that measure biological signals, electrocardiograms, temperature, pressure (5, 6), organic amplifier systems (7), high-sensitivity pressure sensors (8), and ultrathin and imperceptible devices (9, 10).

To measure spatial and temporal temperature gradients of the body, multiple temperature sensors have to be attached on the freely curved surface of the body. One practical solution is to apply multiple discrete temperature sensors to the skin such as thermocouples (11), thermistors (12), or resistive temperature detectors (4, 6, 13) with individual wirings for data readout. Indeed, there are many excellent temperature sensors that exhibit fast response, mechanical flexibility, physiological stability, and/or high sensitivity (4, 6, 13). For example, the thermal sensors using metals as resistors exhibit the change of resistivity less than 1% for the thermal change of 5 °C (6, 13), which can be perfectly resolved by a high-precision electronic circuit. To realize scalable designs for multipoint measurements and/or to ensure sufficient accuracy of temperature measurement on dynamically moving objects due to strain-induced performance changes of sensors, however, it is important to significantly increase change of resistivity, ideally up to several orders-of-magnitude change. Although line-of-sight–based techniques including infrared thermographs and thermotropic liquid crystals (14) are capable of spatial temperature mapping, they require separation between the sensor and target object and, therefore, are unsuitable for implanted devices.

Alternatively, positive temperature coefficient (PTC) polymers (15) have been used to fabricate mechanically flexible

Significance

We have successfully fabricated very unique ultraflexible temperature sensors that exhibit changes in resistivity by six orders of magnitude or more for a change in temperature of only 5 °C or less. Our approach offers an ideal solution to measure temperature over a large area with high spatial resolution, high sensitivity of 0.1 °C or less, and fast response time of 100 ms. Indeed, such a large change of resistivity for our sensors can significantly simplify the readout circuitry, which was the key to demonstrate, to our knowledge, the world's first successful measurement of dynamic change of temperature in the lung during very fast artificial respiration. Furthermore, we have demonstrated real-time multipoint thermal sensing using organic transistor active-matrix circuits.

Author contributions: T.Y., Y.I., Y.T., J.R., K.M., T.M., M.S., W.V., T. Sekitani, and T. Someya designed research; T.Y., Y.I., Y.T., J.R., M.K., T.W., and K.Y. performed research; T.Y. contributed new reagents/analytic tools; T.Y., Y.I., Y.T., J.R., T.W., and K.Y. analyzed data; and T.Y., Y.I., J.R., M.K., and T. Someya wrote the paper.

The authors declare no conflict of interest.

This article is a PNAS Direct Submission.

[1]T.Y. and Y.I. contributed equally to this work.

[2]To whom correspondence may be addressed. Email: yokota@ntech.t.u-tokyo.ac.jp or someya@ee.t.u-tokyo.ac.jp.

This article contains supporting information online at www.pnas.org/lookup/suppl/doi:10.1073/pnas.1515650112/-/DCSupplemental.

temperature sensors that exhibit orders-of-magnitude changes in resistivity over just a few degrees (16). Extraordinarily large resistivity changes can eliminate the need for per-pixel amplification circuitry, as the output signal of the sensor can be directly multiplexed and fed to external recording equipment, ultimately reducing device complexity and manufacturing costs. The PTC effect in conductive-filled polymers results from an increase in the specific volume as the temperature increases, typically during progression through the melting point of crystalline regions (17, 18). For this reason, resistivity is changed drastically by change in temperature for only a few degrees. However, very few polymer PTC materials with sensitivity near physiological temperatures have been demonstrated, and have yet to be fabricated in highly flexible geometries. Besides flexibility and multipoint measurement requirements, each sensor has to exhibit high sensitivity (<0.1 °C) near body temperatures, fast response time (less than 100 ms), and cyclic repeatability. This work demonstrates a highly tuned polymer composite that changes six orders of magnitude over less than 5 °C near body temperature with high cyclic stability. To the best of the authors' knowledge, no other temperature sensors, either rigid or flexible, organic or inorganic, simultaneously exhibit these qualities—less than 0.1 °C sensitivity, cyclic stability near 37 °C, easily processable, with low-complexity readout circuitry. These properties will enable a wide range of medical and nonmedical devices. Competing inorganic devices require complex postamplification of low signals, which complicates readout and the device architecture. Specifically, the need for per-pixel amplification limits the proliferation of simple medical sensors that lend themselves to continued miniaturization, low power utilization, and wireless addressability. Competing organic devices suffer in terms of repeatability, commonly exhibiting less than 100 stable thermal cycles (16, 19, 20). This work presents an important step toward the realization of implantable and wearable devices that are sensitive, cyclically stable, and processable.

Results

To prepare polymer PTC composites, which are simply referred to as copolymer with filler, graphite particles (2–3-μm diameter) are added as conductive fillers to acrylate copolymers. The fabrication process can be seen in *Methods* and *SI Appendix*, Figs. S1 and S2. A photograph and atomic force micrographs of the copolymer with filler film are shown in Fig. 1 *A* and *B*, respectively. With increasing concentration of graphite, the resistivity suddenly decreases to 2×10^4 Ωcm at 10 wt % graphite, which is considered the threshold concentration for percolation conduction (21), and remains relatively constant above 10 wt % (*SI Appendix*, Fig. S3). Indeed, optical microscopic images of the copolymer with filler film surfaces exhibit significant changes at the graphite concentration of 10 wt % (*SI Appendix*, Fig. S4). To ensure the graphite concentration far beyond the threshold, 25 wt % graphite is added to polymer matrix for all of the samples, unless otherwise specified.

Before adding graphite, semicrystalline acrylate copolymers are fabricated by polymerization of two acrylate monomers with different alkyl sidechain lengths. Butyl acrylate with a 4-carbon sidechain and octadecyl acrylate with an 18-carbon sidechain are polymerized in compositions of 37, 48, 54, 61, 78, and 100 mol % OA. These materials without graphite are referred to as copolymers without filler. Alkyl acrylate monomers are widely used in the skin care industry and after polymerization have low toxicity (22).

The electrical characteristics of films made of the copolymers with filler are shown in Fig. 1*C*. The sensing temperature, which is defined as the point of maximum slope of the resistivity vs. temperature curve, is moved systematically from 25 °C to 50 °C by changing the mixing ratio. The melting points as determined by DSC endotherms (Fig. 1*D*) are plotted in Fig. 1*E* as a function of octadecyl acrylate ratio. The melting point of poly(octadecyl acrylate) is 50 °C, and that of acrylate copolymers decreases linearly from 50 °C to 30 °C when the concentration of octadecyl acrylate decreases from 100 to 37 mol %. The melting points, as determined by the peak of the DSC endotherm, show almost identical behavior for the copolymers with and without filler (difference of less than 6%) when the mixture ratio changes (Fig. 1*E* and *SI Appendix*, Fig. S5). The melting point is decreased by 0.3 °C per 1 mol % change in monomer composition. The PTC effect arises from an increase in specific volume during progression through the melt, and so density is measured by a fixed volume expansion method and plotted in Fig. 1*F* as a function of temperature. Density decreases by ~5% when heated above the melt temperature due to expansion of the polymer matrix as it transitions from semicrystalline to amorphous.

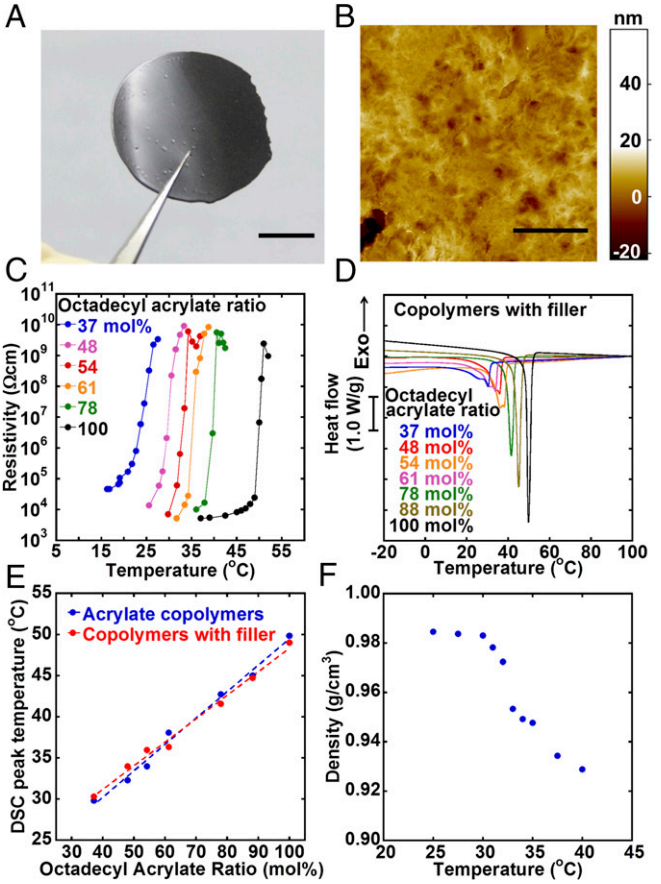

Fig. 1. Characteristics of tunable temperature sensors with high sensitivity. (*A*) Photograph of a film of copolymer with graphite filler. (Scale bar, 1 cm.) (*B*) AFM image of the surface of a film of copolymer with filler at 26 °C. (Scale bar,10 μm.) (*C*) Temperature dependence of the resistivity of the copolymer with filler with various comonomer compositions. Control of the sensing temperature of OA/methyl acrylate copolymers with filler is achieved by changing the mol ratio of OA from 37% to 100%. (*D*) The DSC melt endotherms of the copolymers with filler. The peak temperature is raised by the increased mol ratio of OA. (*E*) Comparison of the peak temperature for the DSC melt endotherms of the acrylate copolymers and copolymers with filler. (*F*) The density of an acrylate copolymer was measured by the fixed volume expansion method. Expansion of the polymer matrix during a melt transition results in a decrease in polymer density.

We systematically examine the stability of ultraflexible temperature sensors, namely, thermal cycling tests, stability in saline, and bending tests. The structure of the sensor can be seen in Fig. 2*A* (*Inset*) and it is referred to as the lateral-type sensor. The copolymer with filler with 54 mol % octadecyl acrylate and 25 wt % graphite is printed through stencil masks and the effective sensing area is 1 × 3 mm^2. The copolymer with filler has a melting point of 36 °C as measured by DSC, whereas the sensors exhibit the highest sensitivity

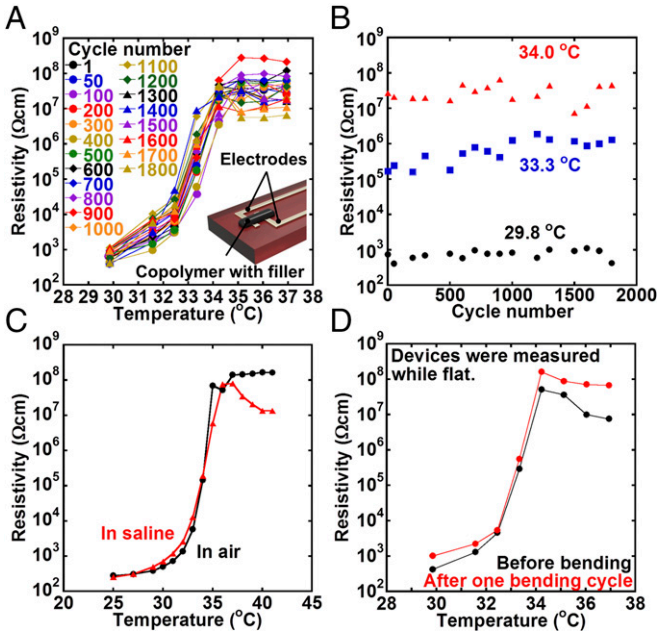

Fig. 2. Cyclic, mechanical, and environmental stability of physiological temperature sensors. (*A*) Heat cycling test for a temperature sensor with 54.0% OA with a lateral structure. Each cycle comprises two steps: heating from 29.8 °C to 37.0 °C and cooling from 37.0 °C to 29.8 °C. (*B*) The temperature dependence of the resistivity of the temperature sensor with a lateral structure. Black circles, blue squares, and red triangles represent resistance values of 29.8 °C, 33.3 °C, and 34 °C, respectively. (*C*) Electrical characteristics of the temperature sensor with a 1-μm-thick parylene passivation layer. Black circles and red triangles represent the characteristics in atmosphere and saline, respectively. (*D*) Flexibility of the temperature sensor. Black and red dots represent the initial resistivity and the resistivity after bending to a radius of 700 μm, respectively. Devices were measured while flat.

near 34 °C. The melting of crystalline domains begins ∼15 °C below the peak of the endotherm.

Cyclic stability was evaluated by heating from 29.8 °C to 37.0 °C for 1,800 thermal cycles while monitoring resistivity. The sensors maintain at least a four-order-of-magnitude change in resistivity even after 1,800 thermal cycles, as shown in Fig. 2*A*. At this time, the noise limit of our measurement setup is about 10^8 Ωcm. Using the same data, resistivities measured at 34 °C, 33.3 °C, and 29.8 °C are plotted in Fig. 2*B* as a function of the number of thermal cycles. The repeatability has been significantly improved in comparison with previously reported PTC-based sensors, which typically show 100 cycles or less. Characteristics of a full thermal cycle are shown in *SI Appendix*, Fig. S6. When heated through the entire melt transition, the temperature sensor exhibits a 1–2 °C hysteresis (*SI Appendix*, Fig S6*A*). Small temperature changes (around 0.2 °C), however, result in a very minor hysteresis (*SI Appendix*, Fig. S6*B*).

High cyclic thermal stability has been achieved due to a previously unidentified device geometry, which will be discussed in this paragraph, and the stability of the material itself, which will be described in the next paragraph. Many previously reported devices have used a vertical structure where the polymer PTC film is sandwiched between two electrodes (denoted as the vertical-type sensor). Here, we demonstrate a lateral-type sensor where the polymer PTC is printed across two neighboring electrodes (16, 23). Both sensor types exhibit similar initial resistivity changes of six orders of magnitude over a temperature change of only 4 °C. The equilibrium stability of both was measured in a thermostat chamber which can be susceptible to temperature fluctuations due to the circulation of water. As a result, the resistance of the device has a slight fluctuation (0.7 MΩ) around 32 °C (*SI Appendix*, Fig. S7), from which the sensitivity is estimated to be less than 20 mK. During thermal cycling, significant degradation in sensitivity is observed for the vertical-type sensor after ∼100 thermal cycles (*SI Appendix*, Fig. S8 *A* and *B*). To quantify the negative temperature coefficient effect for the lateral structure, we heated the device at 35 °C for over 12 h, which resulted in a large decrease in resistivity (*SI Appendix*, Fig. S9). Conversely, devices with the lateral structure did not exhibit a resistivity decrease after heating at 100 °C for 1 h (*SI Appendix*, Fig. S10). One of the possible reasons to explain the improved repeatability is that strains induced by the top electrode of vertical-type sensors under thermal cycles can be avoided in the lateral-type sensors.

Surface and bulk morphology of our copolymer with filler (54 mol % octadecyl acrylate) was characterized via atomic force microscopy (AFM), X-ray diffraction (XRD), and DSC. First, the surface morphology of the acrylate copolymers films and copolymer with filler films is observed by AFM with changing temperature. At temperatures above the melting point, the surface becomes very flat with no distinctive morphology (*SI Appendix*, Figs. S11 and S12). After the first cycle the surface morphology is dramatically changed (*SI Appendix*, Fig. S13 *A* and *B*), but there is no significant change after 1,000 cycles (*SI Appendix*, Fig. S13). Second, the acrylate copolymers without graphite films are characterized by XRD while thermally cycled (*SI Appendix*, Fig. S14). The XRD peak relates to the crystal region that disappears at temperatures above the melting point, and repeatedly appears at the same position when the temperature decreases below the melting point. Third, cyclic measurement of the melting endotherm by DSC shows a stable peak height and peak temperature after the initial thermal cycle (*SI Appendix*, Fig. S15). All of the above results demonstrate stability of the acrylate copolymers semicrystalline morphology after thermally cycling.

To apply the device for implantable electronic applications, the ultraflexible temperature sensors are encapsulated using a 1-μm-thick parylene C coating. The sensor is then directly immersed in saline and the resistivity is measured while changing temperature and compared with that in air (Fig. 2*C*). It is of note that this ultraflexible sensor operates in aqueous environment with only a simple parylene passivation layer, which shows a low water vapor transmission rate of 90 g/m^2 per day and oxygen transmission rate of 2,100 mL/m^2 per day. Due to high oxygen sensitivity, a simple parylene layer does not exhibit sufficiently low gas permeability for the encapsulation of organic PN diodes (24).

In addition, mechanical flexibility is important for in vivo use and is examined by subjecting the sensor films to different bending radii (*SI Appendix*, Figs. S16 and S17). The ultraflexible temperature sensor comprises a 12.5-μm-thick polyimide substrate, 50-nm-thick laterally spaced gold electrodes, and a 12.5-μm-thick copolymer with filler film. The device is bent to a radius of 700 μm and returned to the flat state, and resistivity is measured before and after bending (Fig. 2*D*). The change in thermal response is very small, showing that the device can be bent without causing mechanical damage. Also, the device does not show mechanical damage after 200 cycles of bending to 1-mm radius (*SI Appendix*, Fig. S18). If the sensor is heated above the melting point while under bending stress, a bending radius smaller than 3.5 mm causes small performance changes (*SI Appendix*, Fig. S16) due to deformation of the film of copolymer with filler.

For measuring spatial temperature gradients, a 12 × 12 organic active matrix with polymer PTC sensor pads is fabricated on a polyimide substrate (Fig. 3). The gate dielectric consists of an anodized aluminum oxide layer (9) and a phosphonic acid self-assembled monolayer (SAM) (25). A 30-nm-thick dinaphtho[2,3-b:29,39-f] thieno[3,2-b]thiophene (DNTT) is used as an air-stable organic semiconductor to form a channel layer (26) (*SI Appendix*, Fig. S19). The transistors exhibit a mobility of 2.2 cm^2/Vs and a large on–off ratio of over 10^8. This transistor has a large W/L (W = 15,000 μm, L = 9 μm) for achieving a large on-current of over 3 mA with a 3-V operation voltage (*SI Appendix*, Fig. S19*E*).

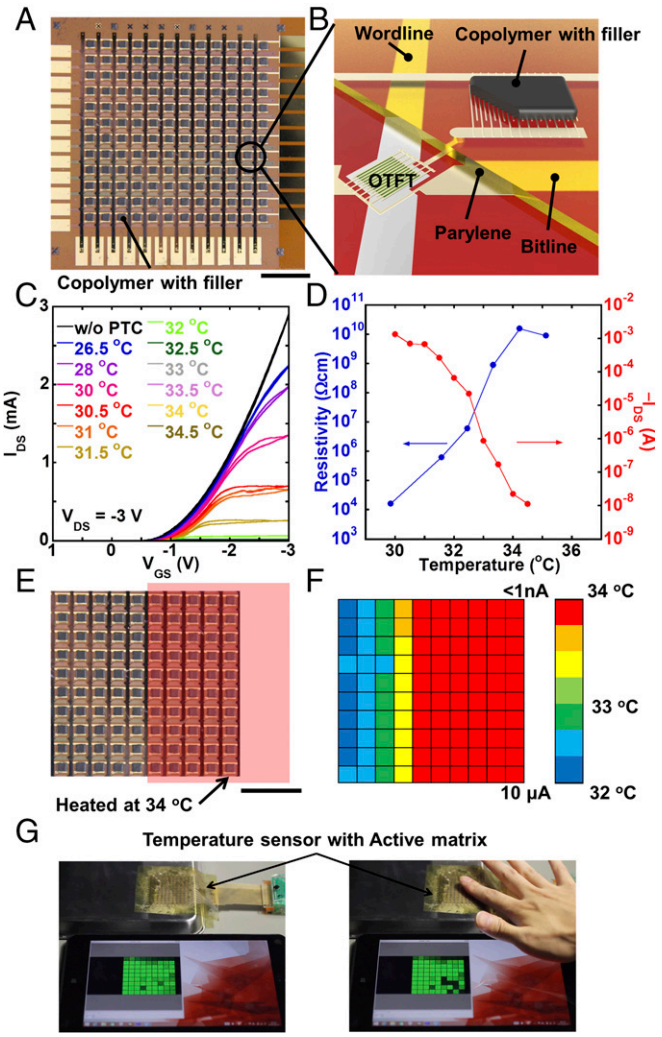

Fig. 3. Flexible temperature sensor sheet for large-area temperature mapping. (*A*) Picture of our flexible temperature sensor sheet. (Scale bar, 1 cm.) (*B*) Cross-sectional illustration of a flexible large-area active-matrix sensor with 12 × 12 temperature pixels. (*C*) Temperature dependence of the electrical characteristics after the integration of the temperature sensor and organic transistor. (*D*) Temperature dependence of the resistivity of the temperature sensor and the on-current of the organic transistor with the temperature sensor. (*E*) Area of a flexible temperature sensor sheet heated to 34 °C. (Scale bar, 1 cm.) (*F*) The spatial temperature gradient when a heated object is placed on the sensing sheet. (*G*) Real-time measurement of the temperature distribution. (*Left*) Temperature mapping before touching. (*Right*) Temperature mapping after touching the sensor sheet with a finger.

Fig. 3*C* shows the characteristics of an individual sensor cell comprising a transistor and temperature sensor. The temperature sensor is connected to the source electrode of the organic transistor. The resistivity of the temperature sensor is gradually increased with increasing temperature, which causes the drain current (I_{DS}) to gradually decrease with increasing temperature (Fig. 3*C*). Fig. 3*D* shows the temperature dependence of the on-current and resistance of the temperature sensors. When the temperature increases from 30.0 °C to 34.5 °C, the on-current decreases from 1 mA to 10 nA, showing a large change (over 10^5) of current for the integrated devices. It should be noted that organic transistors with DNTT channel layers show negligibly small changes when heated to 40 °C (27).

Spatial temperature mapping is demonstrated by placing the sensor matrix on a heat sink (bulk steel) while the right half of the sensor matrix is maintained at 34 °C by a rubber heater sheet, and the room temperature is maintained at 30 °C. Fig. 3 *E* and *F* shows a top-view photograph of the sensor matrix with the heated area (marked by red) and the corresponding current map, respectively. All of the 100 temperature sensor cells on the active-matrix array are functional and the temperature gradients have been measured successfully. The resolution of the temperature gradients is about 5 mm due to thermal diffusion, which is slightly larger than the pixel pitch. Real-time temperature mapping is also demonstrated (Fig. 3*G* and Movie S1). When we touched the temperature sensor by finger, temperature was increased and current was decreased (green and black pixels represent large and small current, respectively).

Additionally, these ultraflexible sensors are able to sense small physiological temperature changes. As shown in Fig. 4, an ultraflexible sensor with the total thickness of 38.5 μm is directly placed on a rat's lung and temperature is monitored. Fig. 4 *A* and *B* shows the experimental setup and the device structure, respectively. The sensor is covered by a 1-μm-thick parylene passivation layer, which is important to ensure stable operation in water for over 5 h (*SI Appendix*, Fig. S20). In this experiment, the ultraflexible sensor is placed between two lobes of the lung and the temperature change over time is observed due to respiration (Fig. 4*C* and Movie S2). Fig. 4*D* shows the temperature change and displacement of the lung during breathing. Temperature changes of ∼0.1 °C were observed with the same period as breathing, without the sensor causing physical damage to the lung or restricting movement of the lung tissue (Fig. 4*D*). This result is consistent with the temperature measurement by infrared camera (*SI Appendix*, Fig. S21). Assuming that the lung has a specific heat of 0.83 cal/g°C, weight of 4 g, surface area of 0.3 m^2, respiratory track volume of 2 mL (28), and breathes 100 times, the amount of heat exchange is calculated to be 2.5 W/m^2. To rule out mechanical deformation as the source of data, the sensor is also applied to an explanted lung while artificially respirated at room temperature (*SI Appendix*, Fig. S22*A*). When the explanted lung was artificially respirated at the same temperature as the environment (25 °C) no resistivity changes were observed in the same sensor, indicating a high degree of insensitivity to mechanical deformation (*SI Appendix*, Fig. S22*B*). We further confirmed the pressure insensitivity of our temperature sensor in the high-temperature region when applying loads as high as 200 Pa (*SI Appendix*, Fig. S23). By fabricating a 5 × 5 temperature sensor array, heat localization on the lung is also demonstrated (Fig. 4 *E* and *F*).

It is also of note that fast temperature response has been successfully demonstrated. When the rat lung is respirated artificially at the breathing rate of 30 and 60 beats per minute (bpm), the temperature response is sufficient to measure each breath (*SI Appendix*, Fig. S24 and Movies S3 and S4), indicating a response time faster than 100 ms. Such a high-speed response becomes possible with reducing the thickness of films of copolymer with filler from 100 to 25 μm. Indeed, a temperature sensor with the thickness over 100 μm could not follow the change of lung temperature (*SI Appendix*, Fig. S25). The decrease in the thickness of the device can reduce the thermal mass and therefore improve the response time.

Discussion

Precise melt temperature tuning is important for realizing multiple human applications, as physiological temperatures range from 32 °C at the fingertips to over 42 °C in the core during hyperpyrexia (29). The sensing temperature can be controlled from 30 °C to 50 °C with changing the mixture ratio of the two acrylate monomers, and the sensing temperature is able to be precisely controlled (within 0.15 °C) if the monomer composition is controlled to within 0.1% of the expected mass values, as shown in *SI Appendix*, Fig. S26. The polydispersity index (PDI) as measured by gel permeation chromatography (GPC) (HLC-8320GPC, Tosoh Corporation) exceeded 2.5 for all samples tested, and indicates a high degree of inhomogeneity in chain molecular weight. Despite this large PDI the width of the melt transition spans less than 15 °C and the peak

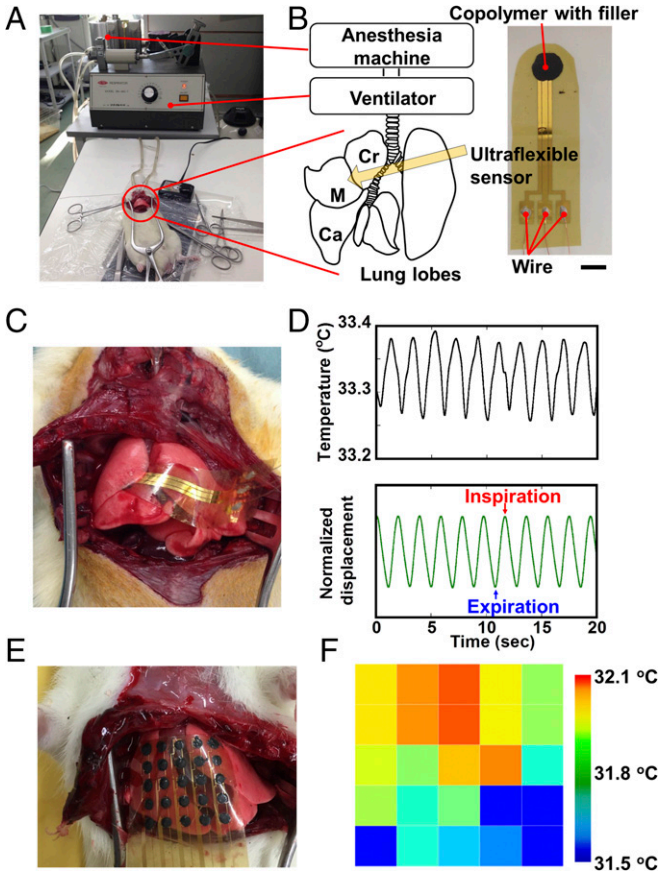

Fig. 4. Measurement of lung temperature during respiration (*A*) Setup of the animal experiments. A median sternotomy was conducted to expose the lung during artificial respiration. (*B*) The temperature sensor (*Left*) was inserted between the cranial lobe (Cr) and median lobe (M) of the right lung during artificial respiration. (Scale bar, 5 mm.) (*C*) Temperature measurement of the respirated lung as heat is exchanged between the lung tissue and air. (*D*) Time course of the temperature of the living lung. (Black: temperature output from the sensor, green: displacement of the lung surface.) The lung temperature periodically fluctuated due to the heat exchange in synchronization with breathing. The inspiration and expiration caused the respective decrease and increase in temperature. (*E*) Temperature mapping measurement of the lung by using a 5 × 5 array of temperature sensors. (*F*) Temperature mapping of the rat lung.

temperature is highly repeatable over multiple syntheses, which is difficult to achieve with main chain crystallizing polymers. Thus, a simple method of tuning the sensing temperature is established which does not rely on changing the polymer molecular weight which is sensitive to the PDI, and is the method used in almost all previous PTC devices (16, 30).

It is noteworthy that precise control over sensing temperature is established in the physiological regime, as the vast majority of previous PTC work has focused on polymers which crystallize along the backbone, including polyethylene and polyethylene oxide. This form of crystallization requires modifications to the molecular weight of polymer chains to change melt temperature, which presents challenges in synthesizing polymers with precise melt temperature control below 70 °C. However, by using polymer sidechain crystallization, whose melt temperature is less sensitive to variations in polymer molecular weight (*SI Appendix*, Fig. S27) and large PDIs, we circumvent many of the challenges in reliably synthesizing polymers with precise melt temperature control. Long alkyl chains tend to crystallize, and longer alkyl chains tend to melt at higher temperatures than short sidechains. Thus, the tuning of the comonomer ratio of a long and short sidechain monomer allows for precise control of the melt temperature (31). In fact, when we change the molecular weight from 250,000 g/mol to 170,000 g/mol by changing the ratio of photoinitiator, the melt temperature does not vary more than 0.17 °C (*SI Appendix*, Fig. S28).

One of the possible explanations for the high repeatability demonstrated in this work is that long alkyl sidechains prevent particle migration through many chain entanglements. Indeed, Long et al. have shown that the structures of branched chain polymers significantly affect the flow properties in the melting phase because of entanglements of the chain segments (32).

In the present design, our passive-type temperature sensor array features 5 × 5 pixels with a 5-mm pitch. Considering the density of capillary vessels, sweat glands, and the heat-transfer coefficient of moist tissue, sensors arrays with 2–3-mm pitch would be most suitable for recording thermal events (33). Additionally, a porous mesh-like structure is needed to allow for natural perspiration. These types of devices are important areas of future research, and are expected to enable long-term thermal mapping in soft tissue.

Methods

Semicrystalline Polymer. Octadecyl acrylate (OA), butyl acrylate (BA), and photoinitiator 2,2-Dimethoxy-2-phenylacetophenone (DMPA) (Sigma-Aldrich Corporation) were used without purification. Tetrahydrofuran (THF) was purchased from Wako Pure Chemical Industries. Alkyl acrylate monomers OA and BA were mixed in varying compositions with 1.0 wt % DMPA and dissolved in an additional 100 wt % THF. Polymerization was carried out via exposure to 365-nm UV light (UVL-28 EL series, 4 W) for 1 d between two glass slides to avoid exposure to oxygen. The organic solvent was then removed under vacuum in a desiccator for 1 d.

Copolymer with Filler Paste and Film. The synthesized semicrystalline polymer was mixed with graphite (2–3 μm, Furuuchi Chemical Corporation) in a weight ratio of 3:1 polymer:graphite under heat using a magnetic stirrer for 1 d, and in a planetary centrifugal vacuum mixer (THINKY MIXER ARV-310, Thinky Corporation) for 10 min at 1,000 rpm. The copolymer with filler was then pressed between two glass slides at 10 N for 5 min at 40 °C to form copolymer with filler films, using a 25-μm-thick polyimide film (UPILEX-25S, Ube Industries, Ltd.) as a spacer. Finally, the copolymer with filler film was delaminated from glass.

Ultraflexible Temperature Sensor. For ultraflexible temperature sensors with vertical orientation, the polymer copolymer with filler film was sandwiched between two gold electrodes that were deposited on 12.5- or 50-μm polyimide film substrate. The copolymer with filler paste was then hot-pressed at 40 °C with 10 N of pressure for 10 min. Printed temperature sensors were fabricated by mixing 10 wt % THF or 4-methyl-2-pentanone (Wako Pure Chemical Industries) with the copolymer with filler paste and printing on interdigitated gold electrodes through a polyimide or metal mask.

Thin-Film Transistors. The 100-nm-thick Al gate electrode was formed by thermal evaporation using a shadow mask. The aluminum oxide gate dielectric layer was formed by potentiostatic anodization under ambient conditions. A 0.01-M citric acid monohydrate ($C_6H_8O_7{\cdot}H_2O$) electrolyte was prepared using ultrapure (18 MΩ cm) water. The contacted gates were then immersed in the electrolyte to form the working electrode (anode), and a platinum foil served as the counter electrode. After forming the aluminum oxide layer, we activated the surface of the aluminum oxide in oxygen plasma (3 min at 150 W), and dipped the substrate into a 5-mM solution of the n-tetradecyl phosphonic acid SAM for 16 h to form the 2-nm-thick SAM. Then, a 30-nm-long DNTT layer was evaporated through a shadow mask as an organic channel layer, and a 50-nm-thick length of gold was evaporated through a shadow mask as source and drain electrodes with W = 15,000 μm and L = 9 μm for single transistors.

Active-Matrix Temperature Sensing Sheet. The 12 × 12 active-matrix organic transistor used the same fabrication method as the single transistor. We used 1 μm of parylene C (Daisan Kasei Co. Ltd.) formed by chemical vapor deposition (CVD) to separate the organic transistor matrix from the temperature sensor layer. A green laser marker system (T-Centric SHG Laser Marker, Keyence) was used to make via holes to the underlying transistors through the parylene. We evaporated 100-nm-thick interdigitated gold electrodes with 50-μm pitch through a shadow mask, and copolymer with filler paste was printed through a mask while the substrate was heated to 50 °C.

Device Characterization. The electrical characterization of transistors and active-matrix sensing sheets was performed with a semiconductor parameter analyzer (Agilent B1500A) under ambient laboratory conditions. Optical images were recorded with a Keyence VK-9710 UV laser microscope. AFM images of polymer and copolymer with filler film surface morphologies were characterized using an Agilent 5500 AFM/SPM (Agilent Technology). XRD measurements were performed using Smart Lab (Rigaku).

Animal Experiment. A rat was prepared for a tracheostomy by anesthetization with 2–3 isoflurane at a temperature of 25 °C and humidity of 100% (SN-487–0T, Shinano Seisakusho Co. Ltd.) while under mechanical ventilation (SN-480–7, Shinano Seisakusho Co., Ltd.). The preset breathing rate and tidal volume were controlled within normal limits by the mechanical ventilation system. The lung was exposed by median sternotomy, and the ultraflexible temperature sensor placed between the right upper lobe (Cr) and the right middle lobe (M) (Fig. 4*B*). The sensor was fabricated on a 12.5-μm polyimide film substrate and a 1.5-μm-thick parylene C layer was formed as a passivation layer using the CVD machine (LABCOTER PDS2010, Specialty Coating Systems). The temperature was evaluated using voltage change, which was measured under constant current conditions. The displacement of the lung was simultaneously measured using a laser displacement meter (IA-030&IA-1000, Keyence), and we estimated the breathing cycle. All data were recorded by the data logger (PowerLab 16s, AD Instruments Limited) with accurate temporal synchronization. During the experiments, the rat temperature was controlled at 37 °C by a heater (Magami Denshi Co. Ltd.: MP-914N). All animal-based experiments were approved by the Ethics Committee of the University of Tokyo.

The windpipe and lung of a rat were explanted and artificially respirated under constant temperature (25 °C) conditions. The temperature change and the displacement of the lung was measured for 10 min after the temperature of the lung had stabilized.

ACKNOWLEDGMENTS. The authors are indebted to Prof. Takanori Fukushima (Tokyo Institute of Technology), Dr. Takashi Kajitani, Dr. Fumitaka Ishiwari, and Dr. Kazunori Kuribara [University of Tokyo, presently National Institute of Advanced Industrial Science and Technology (AIST)], Naoji Matsuhisa (University of Tokyo), and Hiroaki Jinno, Tatsuya Nakamura, and Hiroki Kitanosako for fruitful discussions. Research at The University of Texas at Dallas by W.V. is partly supported by the National Science Foundation Graduate Research Fellowship Grant 2013155309. This work was supported by Japan Society for the Promotion of Science (JSPS) KAKENHI Grant 30723481.

1. Arora N, et al. (2008) Effectiveness of a noninvasive digital infrared thermal imaging system in the detection of breast cancer. *Am J Surg* 196(4):523–526.
2. Shevelev IA (1992) Temperature topography of the brain cortex: Thermoencephaloscopy. *Brain Topogr* 5(2):77–85.
3. Bagavathiappan S, et al. (2009) Infrared thermal imaging for detection of peripheral vascular disorders. J Med Phys 34(1):43–47.
4. Kim DH, et al. (2011) Epidermal electronics. *Science* 333(6044):838–843.
5. Viventi J, et al. (2011) Flexible, foldable, actively multiplexed, high-density electrode array for mapping brain activity in vivo. *Nat Neurosci* 14(12):1599–1605.
6. Xu L, et al. (2014) 3D multifunctional integumentary membranes for spatiotemporal cardiac measurements and stimulation across the entire epicardium. *Nat Commun* 5:3329.
7. Khodagholy D, et al. (2013) In vivo recordings of brain activity using organic transistors. *Nat Commun* 4:1575.
8. Schwartz G, et al. (2013) Flexible polymer transistors with high pressure sensitivity for application in electronic skin and health monitoring. *Nat Commun* 4:1859.
9. Kaltenbrunner M, et al. (2013) An ultra-lightweight design for imperceptible plastic electronics. *Nature* 499(7459):458–463.
10. Fuketa H, et al. (2014) 1 μm-thickness ultra-flexible and high electrode-density surface electromyogram measurement sheet with 2 V organic transistors for prosthetic hand control. *IEEE Trans Biomed Circuits Syst* 8(6):824–833.
11. Imran M, Bhattacharyya A (2006) Effect of thin film thicknesses and materials on the response of RTDs and microthermocouples. *IEEE Sens J* 6(6):1459–1467.
12. Park IJ, et al. (2012) Fabrication of amorphous InGaZnO thin-film transistor-driven flexible thermal and pressure sensors. *Semicond Sci Technol* 27:105019.
13. Webb RC, et al. (2013) Ultrathin conformal devices for precise and continuous thermal characterization of human skin. *Nat Mater* 12(10):938–944.
14. Gao L, et al. (2014) Epidermal photonic devices for quantitative imaging of temperature and thermal transport characteristics of the skin. *Nat Commun* 5:4938.
15. Shih WP, et al. (2010) Flexible temperature sensor array based on a graphite-polydimethylsiloxane composite. *Sensors (Basel)* 10(4):3597–3610.
16. Jeon J, Lee HBR, Bao Z (2013) Flexible wireless temperature sensors based on Ni microparticle-filled binary polymer composites. *Adv Mater* 25(6):850–855.
17. Luo Y, Wang G, Zhang B, Zhang Z (1998) The influence of crystalline and aggregate structure on PTC characteristic of conductive polyethylene/carbon black composite. *Eur Polym J* 34(8):1221–1227.
18. Meyer J (1973) Glass transition temperature as a guide to selection of polymers suitable for PTC materials. *Polym Eng Sci* 13(6):462–468.
19. Xu XB, Li ZM, Dai K, Yang MB (2006) Anomalous attenuation of the positive temperature coefficient of resistivity in a carbon-black-filled polymer composite with electrically conductive in situ microfibrils. *Appl Phys Lett* 89:032105.
20. Kim GT, Park ES (2008) Thermal reproducibility and voltage stability of carbon black/multiwalled carbon nanotube and carbon black/SnO_2-Sb coated titanium dioxide filled silicone rubber heaters. *J Appl Polym Sci* 109(3):1381–1387.
21. Sumita M, Abe H, Kayaki H, Miyasaka K (1986) Effect of melt viscosity and surface tension of polymers on the percolation threshold of conductive-particle-filled polymeric composites. *J Macromol Sci Phys* 25(1-2):171–184.
22. Zondlo F (2002) Final report on the safety assessment of Acrylates Copolymer and 33 related cosmetic ingredients. *Int J Toxicol* 21(3 Suppl):1–50.
23. Chuang WJ, Chiu WY, Tai HJ (2012) Temperature-dependent conductive composites: Poly(N-isopropylacrylamide-co-N-methylol acrylamide) and carbon black composite films. *J Mater Chem* 22:20311–20318.
24. Someya T, et al. (2005) Conformable, flexible, large-area networks of pressure and thermal sensors with organic transistor active matrixes. *Proc Natl Acad Sci USA* 102(35):12321–12325.
25. Klauk H, Zschieschang U, Pflaum J, Halik M (2007) Ultralow-power organic complementary circuits. *Nature* 445(7129):745–748.
26. Yamamoto T, Takimiya K (2007) Facile synthesis of highly π-extended heteroarenes, dinaphtho[2,3-b:2′,3′-f]chalcogenopheno[3,2-b]chalcogenophenes, and their application to field-effect transistors. *J Am Chem Soc* 129(8):2224–2225.
27. Kuribara K, et al. (2012) Organic transistors with high thermal stability for medical applications. *Nat Commun* 3:723.
28. Whitehead GS, Kimmel EC, Reboulet JE, Still KR (1999) *Pulmonary Function in Normal Rats. No. TOXDET-99-5* (Naval Health Research Center Detachment (Toxicology), Wright-Patterson Air Force Base, OH).
29. Gradisar M, Lack L (2004) Relationships between the circadian rhythms of finger temperature, core temperature, sleep latency, and subjective sleepiness. *J Biol Rhythms* 19(2):157–163.
30. Narkis M, Ram A, Flashner F (1978) Electrical properties of carbon black filled polyethylene. *Polym Eng Sci* 18(8):649–653.
31. O'Leary K, Paul DR (2006) Physical properties of Poly (n-alkyl acrylate) copolymers. Part 1. Crystalline/crystalline combinations. *Polymer (Guildf)* 47(4):1226–1244.
32. Long VC, Guy CB, Hobbs LM (1964) Solution and bulk properties of branched polyvinyl acetates IV—Melt viscosity. *Polymer (Guildf)* 5:517–524.
33. Pennes HH (1948) Analysis of tissue and arterial blood temperatures in the resting human forearm. *J Appl Physiol* 1(2):93–122.